Hybrid Goldstone modes in multiferroic $YMnO_3$ studied by polarized inelastic neutron scattering

S. Pailhès,[1] X. Fabrèges,[1] L. P. Régnault,[2] L. Pinsard-Godart,[3] I. Mirebeau,[1] F. Moussa,[1] M. Hennion,[1] and S. Petit[1]
[1]*Institut Rayonnement Matière de Saclay, Laboratoire Léon Brillouin, CEA-CNRS, UMR 12, CE-Saclay, F-91191 Gif-sur-Yvette, France*
[2]*Institut Nanosciences et cryogénie, CEA-Grenoble, DRFMC-SPSMS-MDN, 17 rue des Martyrs, F-38054 Grenoble Cedex 9, France*
[3]*Institut de Chimie Moléculaire et des Matériaux d'Orsay, Laboratoire de Physico-Chimie de l'Etat Solide, UMR CNRS 8182, Bâtiment 410, Université Paris Sud, F-91405 Orsay Cedex, France*
(Received 13 February 2009; published 7 April 2009)

We used polarized inelastic neutron-scattering measurements to shed light on the spin-lattice quantum entanglement in multiferroic materials. We report an evidence for hybrid elementary excitations made of a mixing between spin waves and phonons, which can be considered as multiferroic Goldstone modes. We argue that the Dzyaloshinskii-Moriya interaction could be at the origin of this hybridization.

DOI: 10.1103/PhysRevB.79.134409 PACS number(s): 75.30.Ds, 71.45.−d, 72.10.Di, 77.80.−e

I. INTRODUCTION

Multiferroics continue to arouse much attention due to their intriguing properties, showing coexisting and strongly coupled ferroelectric and magnetic orders. Actually, this unique property might offer the opportunity to control charges by applying magnetic fields and spins by applying voltages, and in turn to design new multifunctional electronic devices.[1]

At the moment, the microscopic mechanism at the origin of the coupling between the two order parameters remains however unknown. To shed light on this problem, recent studies have been devoted to identify the low-energy excitations—the so-called Goldstone modes[2]—associated with the multiferroic phase. Since the ferroelectric polarization and the magnetization are strongly coupled,[3,4] the multiferroic Goldstone modes are expected to be spin and lattice hybrid excitations called electromagnons.[5–8] While their existence has been theoretically predicted a long-time ago,[9,10] their composite nature as both spin and lattice makes them challenging to observe experimentally.

Due to their dipole electric activity, they first could be detected by optical measurements, especially in different orthorhombic multiferroics, namely, $GdMnO_3$, $TbMnO_3$,[11] $Eu_{0.75}Y_{0.25}MnO_3$,[12] $DyMnO_3$,[13] YMn_2O_5, $TbMn_2O_5$,[14] and $BiFeO_3$.[15,16] However, their magnetic counterpart is still not clearly demonstrated. Moreover, as optical techniques probe the zone center $Q=0$, the dispersion laws and in turn the underlying mechanism responsible for the hybridization are still unknown.

In the following, we focus on the particular case of $YMnO_3$ and report polarized inelastic neutron-scattering experiments proving the existence of such hybrid modes (HMs) in this material. In addition, as neutron scattering allows a global survey of the entire Brillouin zone, we report measurements of their dispersion. These findings are discussed in the framework of the dynamical magnetoelectric coupling theory, where the Dzyaloshinskii-Moriya interaction plays a central role.

$YMnO_3$ undergoes a paraelectric-ferroelectric transition at about 900 K.[15,17] The Mn ions ($S=2$) form a nearly ideal two-dimensional triangular lattice; each Mn ion being connected to another through an oxygen atom located on the same basal plane. The triangular lattice of the Mn spins exhibits strong geometrical antiferromagnetic frustration as evidenced by the high value of the Curie-Weiss temperature of −500 K. Nevertheless, the Mn spin orders in a classical triangular arrangement within the basal plane below the Néel temperature $T_N=75$ K (Refs. 18 and 19) as sketched in Fig. 1(a). The electric polarization lies along the c axis perpendicularly to the Mn-O plane. At T_N, large atomic displacements have been recently reported, leading to a small increase in the electric polarization.[20]

II. EXPERIMENTAL DETAILS

Our neutron-scattering studies were carried out on the 4F1 and IN22 triple axis spectrometers installed, respectively, at LLB-Orphée (Saclay, France) and at the Institute Laue Langevin (Grenoble, France). As we are interested in hybrid modes, it is important to be able to measure separately the spin and dynamic structure factors. This is usually carried out by controlling the spin state of the incident and scattered neutrons, within the longitudinal polarization analysis (LPA) framework.[21,22] This technique offers an efficient way to measure both response functions in separate channels called spin flip (SF) and nonspin flip (NSF). Switching between the two channels is operated by flipping the spin of the scattered neutrons and is thus operated without movements of the sample. According to the magnetic and nuclear neutron-scattering cross sections, selection rules are different for both channels. In the magnetic case, one measures spin fluctuations perpendicular to the wave vector Q. In contrast, the nuclear case probes atomic vibrations parallel to the wave vector Q.

The sample was aligned in the scattering plane (100) and (001) such that the momentum transfer of the form $Q=(H,0,L)$ in units of reciprocal-lattice wave vectors were accessible [see Fig. 1(a)]. All data were obtained with a fixed final wave vector of 2.662 $Å^{-1}$ providing an energy resolution less than 1 meV. Heussler crystals were used as analyzer and monochromator, together with a flipper of Mezei to reverse the spin of the scattered neutrons. The flipping ratio

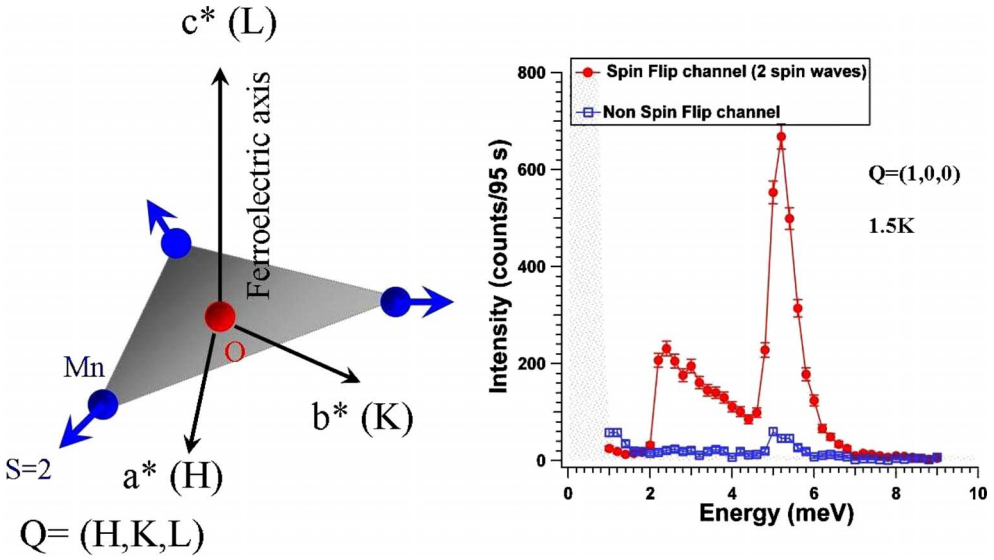

FIG. 1. (Color online) (a) Sktech of the Mn-O plane with the ordered spins ($S=2$) of the Mn ions as observed in the Néel state in hexagonal multiferroics. The reciprocal vectors (a^*, b^*, and c^*) are also depicted. The momentum transfer $Q=(H,K,L)$ is expressed in units of reciprocal wave vectors. (b) Typical measurement of "normal" spin waves at the wave vector $Q=(100)$. The peaks appear only in the SF channel (red open circles) whereas the signal measured in the NSF channel (blue open squares) corresponds to the leak of intensity from the SF channel. Note that the asymmetric profile of the first spin-wave peak could be due to resolution effects.

denoted by R was determined from different nuclear and magnetic Bragg peaks above and below T_N, leading to $R \approx 16$. The amplitude of the leak from the SF channel to the NSF channel is therefore less than $1/R \approx 7\%$ of the SF intensity. Using an unpolarized beam pyrolytic graphite monochromator, we measured a polarization parallel and perpendicular in- and out of plane to the wave vector less than 10^{-2} excluding the presence of chiral terms and of the nuclear-magnetic interference terms.[21,22]

III. EVIDENCE FOR A HYBRID MODE

Previous experiments have shown that below T_N, three almost doubly degenerate spin-wave modes rise up.[18,23,24] At the zone center, these modes are characterized by spin gaps, typical of magnetic anisotropy. This is illustrated on Fig. 1(b), which shows energy scans performed at the wave vector (100) and collected in the Néel state at 1.5 K. The peaks at 2.2 and 5 meV in the SF channel correspond to these gaps. In the NSF channel, we observe tiny peaks corresponding exactly to the expected leak of intensity from the SF channel.

We now move from $Q=(1,0,0)$ to $Q=(0,0,6)$. At this new Q position, one probes the spin components within the basal plane. Figure 2 depicts energy scans at this wave vector in both channels measured above and below T_N. At 150 K, the SF channel [Fig. 2(a)] shows a large magnetic quasielastic signal. This is in agreement with strong spin correlations in the paramagnetic phase arising from the geometrically frustrated Mn moments.[18] Below T_N [Fig. 2(c)], spin-wave modes rise up, but due to selection rules, a single mode at $\omega=\Delta_{SG}=5$ meV is now observed. Δ_{SG} represents the energy required to move the spins out of the basal plane. Its large value reveals a strong in-plane anisotropy. Figure 5(b) shows its temperature dependence (red filled circles). As the magnetic long-range order develops, Δ_{SG} gradually shifts to higher values and reaches its maximum of about 5.3 meV around 40 K.

As shown on Fig. 2(b), the NSF channel shows at 150 K a quasielastic signal as well. Since the nuclear cross-section probes fluctuations along $Q=(0,0,6)$, which is parallel to the c axis, we attribute this nuclear quasielastic signal to relaxational vibrations of the various atoms along this particular direction. Surprisingly at 1.5 K [Fig. 2(d)], an anomalous inelastic peak emerges in the NSF channel. Its energy position and linewidth coincide with the spin wave mode at $\omega=\Delta_{SG}$, pointing out its close connection with the spin subsystem. We note that its intensity is very large, only two times lower than the intensity of the spin wave. Thus, according to the flipping ratio, it cannot be an artifact and can be attributed to a new hybrid (spin and lattice) mode. In the following, we will call this anomalous peak observed in the NSF channel as "nuclear mode."

To understand the temperature dependence of both quasielastic and inelastic contributions, NSF energy scans have been performed at different temperatures around T_N. Figure 3(a) shows the corresponding raw data collected at 80, 60, 40, 25, and 1.5 K. For all temperatures, the quasielastic contribution can be observed around $\omega=0$, while the "nuclear mode" rises at low temperatures only. The intrinsic temperature dependence of these two components is better studied by taking away the detailed balance factor. Indeed, the neutron intensity is proportional to the imaginary part of the susceptibility via the detailed balance factor: $I=(1+\frac{1}{e^{\hbar\omega/k_BT}-1})\chi''$. Figure 3(b) shows the corresponding imaginary part of the lattice susceptibility obtained at 1.5 and 150 K. We observe that the quasielastic contribution basically do not evolve with temperature. Further, we note that the nuclear mode rises upon cooling on the top of the quasielastic signal as a supplementary intensity. By fitting the nuclear mode with a simple

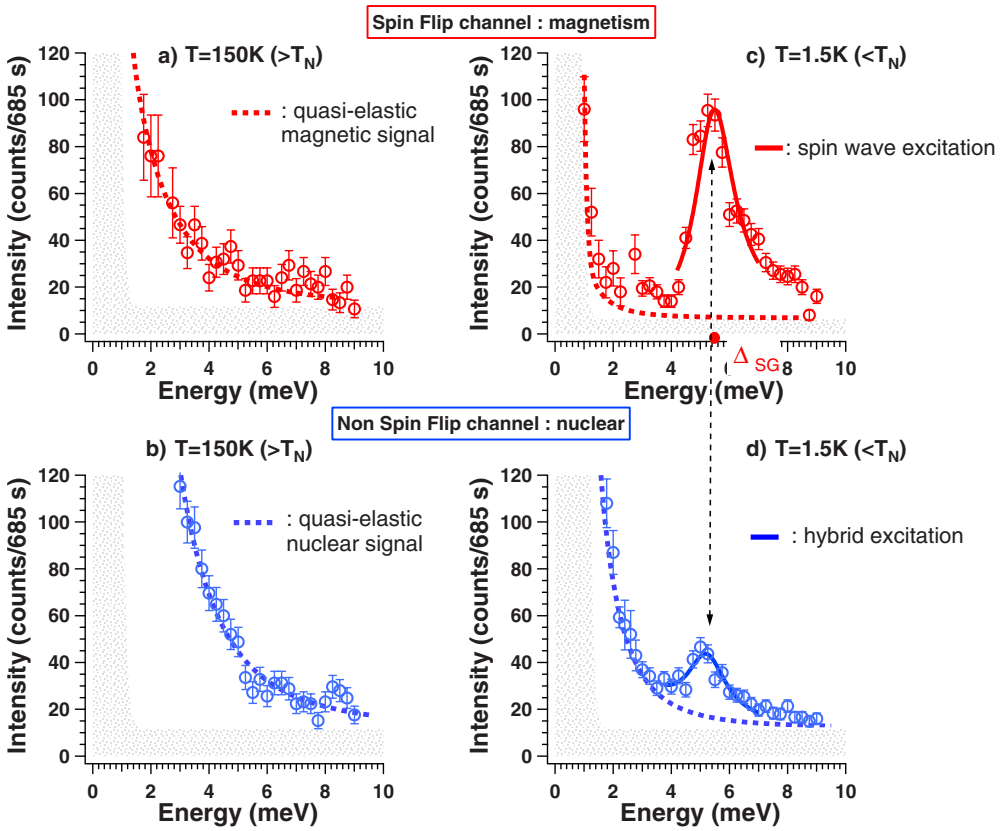

FIG. 2. (Color online) Dynamical magnetic and nuclear changes from the paramagnetic phase to the Néel ordered state. (a)–(d) report energy scans in the SF (red labeled) and NSF (blue labeled) channels at the wave vector $Q=(0,0,6)$ measured in the paramagnetic phase (left column) and in the Néel state (right column). Red and blue lines are fits to the data including the spin waves and the nuclear mode for low-temperature scans.

Lorentzian shape, we determine its characteristic energy reported on Fig. 4(b). Below 40 K, it is found to follow the spin gap value Δ_{SG}, while above 40K, its presence becomes hard to distinguish. To overcome this difficulty, we measured the NSF intensity at $Q=(0,0,6)$ for sampling temperatures for an energy ($\omega=2.2$ meV$\leq\Delta_{SG}$). The data are reported on Fig. 4(a). At this (Q,ω) position, the quasielastic contribution is expected to give a signal proportional to the detailed balance factor. The data can indeed be fitted by this law depicted by a gray line on Fig. 4(a). However, we observe a small deviation from this behavior in the intermediate region surrounding T_N that we attribute to the raising of the nuclear mode starting from the lowest energies. Such measurements allow estimating the energy of the nuclear mode for temperatures higher than 40 K. Figure 4(b) summarizes our results, plotting the spin gap Δ_{SG} and the energy of the nuclear mode as a function of temperature. It shows that the two characteristic energies follow the same temperature dependence from 1.5 K until T_N.

From the data shown on Figs. 2 and 3, we conclude that the hybrid mode is observed with Q along the c axis but not with Q along a^*. As a result, we propose to attribute it to collective vibrations along this particular direction. We note that c is the ferroelectric axis. Moreover, since it is found at a zone center, it corresponds to vibrations within the decoration of the unit cell.

IV. DISPERSION OF THE HYBRID MODE

Now the question is how do such internal motions propagate through the crystal? To address this point, it is essential to determine the dispersion of the hybrid mode by repeating the same measurements for different $Q=(H,0,6)$ with varying H, going from the zone center ($H=0$) to the half of the Brillouin zone ($H=0.5$). Figure 5(a)–5(d) shows the corresponding energy scans for four H values in the SF (red) and NSF (blue) channels.

These data allow to determine the dispersion of the modes which are trivially expected, namely, the spin-wave modes (red points in SF channel on Fig. 5) and the transverse-acoustic phonon (denoted by P on Fig. 5). The dispersion of these modes is reported on Fig. 6 and is consistent with previous unpolarized neutron measurements.

The amazing observation is that the nuclear mode appears for all the four H values in the NSF data, precisely at the same energy positions than the two low-energy spin-waves modes denoted by hybrid mode "HM" on Fig. 5. Its intensity is found to decrease with increasing wave vector. For instance, at $Q=(0.325,0,6)$, it becomes comparable to the expected leak of the intensity from the SF channel. The matching with the spin-wave dispersion for a wide range of wave vectors evidences the close connection with the spin-lattice degrees of freedom. At this step, we conclude that the spin

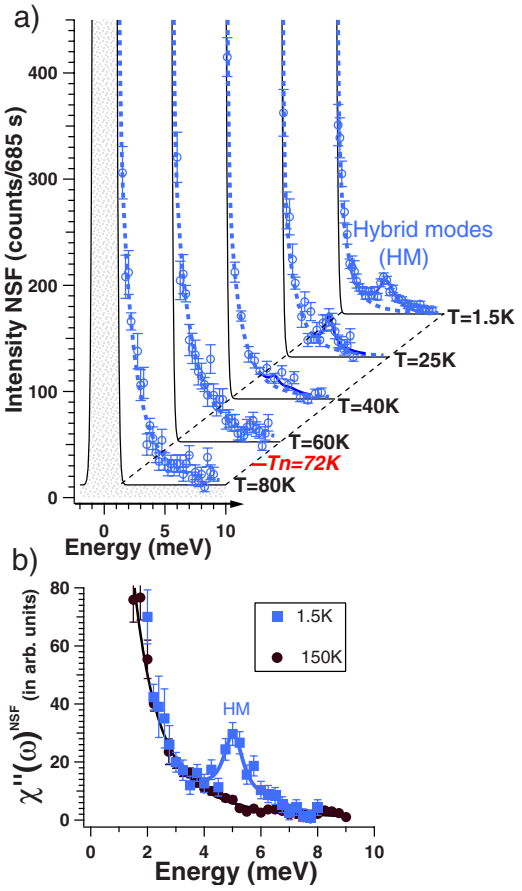

FIG. 3. (Color online) Nuclear mode at the zone center in the Néel phase. (a) Energy scans in the NSF channels at the wave vector $Q=(0,0,6)$ for different temperatures above and below T_N. Below T_N, the additional nuclear excitation or "HMs" starts to form from the 40 K (blue line). (b) Background subtracted and detailed balance factor divided neutron intensity of (a).

wave and the nuclear mode form a single hybrid lattice-spin mode. In other words, the spin-wave excitations are intertwined with nuclear collective vibrations which propagate through the crystal.

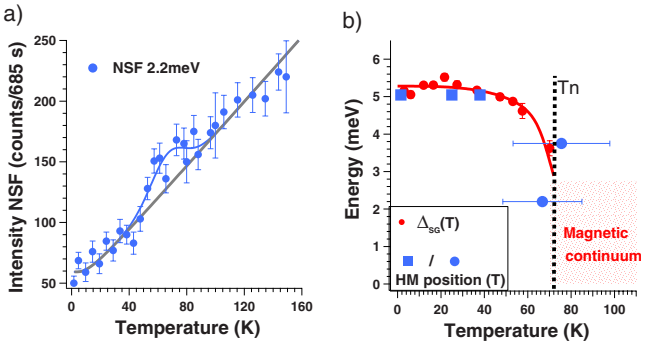

FIG. 4. (Color online) Nuclear mode at the zone center in the Néel phase. (a) Temperature dependence of the NSF inelastic intensity at 2.2 meV. The gray line corresponds to the detailed balance factor. (b) Temperature dependences of the spin gap (red points measured with unpolarized neutrons) and of the nuclear mode (blue points) positions.

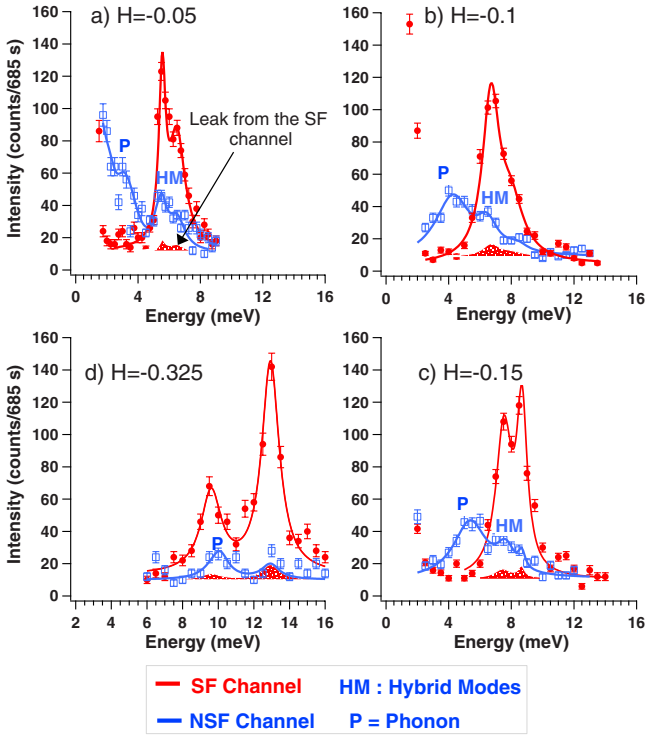

FIG. 5. (Color online) Nuclear and magnetic energy dispersions. Energy scans taken at 1.5 K for different wave vectors $Q=(H,0,6)$ in both SF (full points and red fits) and NSF (open points and blue fits) channels. The H component is indicated in the top left corner of each panel. The dotted line indicates the position of the nuclear mode (see text). The lowest right panel depicts the dispersions of the different low-energy excitations: measured (filled red points) and calculated (dotted red lines) spin-waves, transverse-acoustic phonon (blue square), and hybrid modes (open blue circles).

V. DISCUSSION

The emergence of hybrid modes resulting from the spin-lattice coupling has been mainly discussed in the context of ferrous halides ($FeCl_2$ or $FeBr_2$).[25] Here, the hybridization is caused by a resonant interaction and takes place at the crossing point between bare phonons and spin-waves dispersion. As one moves away from this particular point, the phonon or spin-wave character is restored. In contrast, the hybridization mechanism in the context of multiferroics is very different. First, we note that there is no preexisting phonon mode at high temperature in the energy range of interest (see Fig. 3). Next, we observe the hybrid mode over a large part of the Brillouin zone down to the zone center $H=0$ (see Fig. 7). This itself shows that the long-range properties of the system are affected. As a result, the hybrid multiferroic mode should be considered as a spin wave dressed with atomic fluctuations.

In explaining these findings, we propose to consider a coupling of the spin subsystem with atomic displacements within the unit cell. Note that such static displacements have been observed on entering the Néel phase.[20] This in turn implies a hybridization mechanism with an optical phonon,

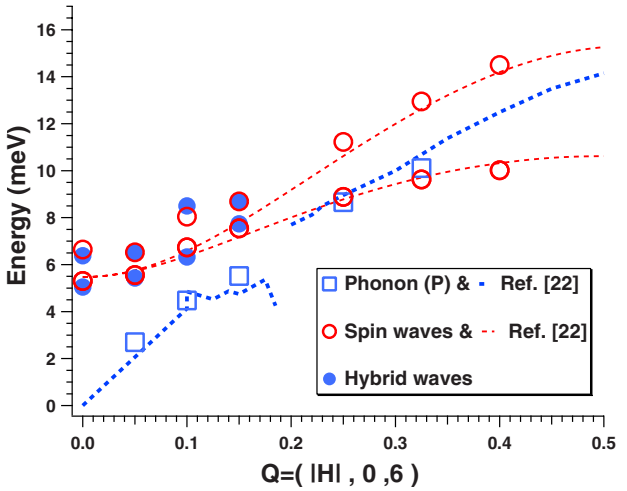

FIG. 6. (Color online) Nuclear and magnetic energy dispersions. Energy scans taken at 1.5 K for different wave vectors $Q=(H,0,6)$ in both SF (full points and red fits) and NSF (open points and blue fits) channels. The H component is indicated in the top left corner of each panel. The dotted line indicates the position of the nuclear mode (see text). The lowest right panel depicts the dispersions of the different low-energy excitations: measured (filled red points) and calculated (dotted red lines) spin-waves, transverse-acoustic phonon (blue square), and hybrid modes (open blue circles).

as in the dynamical magnetoelectric coupling theory developed for orthorhombic $RMnO_3$.[5,6,26] In this scenario, the spin current $J_{ij}=S_i\times S_j$ (defined for neighboring manganese spins S_i and S_j sitting at a distance r_{ij}) plays a crucial role. Owing to the spiral magnetic ordering typical of these materials, J_{ij} acts, via the inverse Dzyaloshinskii-Moryia coupling, as a force pushing the oxygen atom located between adjacent manganese off the Mn-Mn bond. This mechanism gives rise at T_N to an electric polarization $P=r_{ij}\times J_{ij}$ lying within the spiral plane and perpendicular to r_{ij}. The multiferroic Goldstone mode is predicted to be a hybrid mode, rising at Δ_{SG}, and made of a mixing between the optical phonon associated with the oxygen displacement and the spin-wave mode involving spin fluctuations out of the spiral plane. At first glance, this mechanism would not hold in the hexagonal case, since due to the triangular symmetry, the resulting magnetic force experienced by oxygen atoms is zero. Indeed, each oxygen ion is located at the center of a triangle formed by three neighboring Mn ions. The system can however benefit from the Dzyaloshinskii-Moryia interaction by spontaneously moving the oxygen atoms along the c axis. This distortion is expected to create an electric polarization parallel to J_{ij} and is accompanied by a slight rotation of the spins toward the same direction. In that case, the coupled spin and atomic motions look like those of the ribs of an umbrella that would be put up or down (Fig. 5). In close analogy with the orthorhombic case, hybridized spin-lattice Goldstone modes are expected at Δ_{SG}, in agreement with the present results.

To test the validity of this scenario, several predictions have to be further examined. First, the magnetic structure should be characterized by a tiny ferromagnetic moment superimposed on the antiferromagnetic (AF) structure, as sketched in the right panel of Fig. 5 (see also Ref. 27). Calculations of the structure factor show that this effect is best observed for Bragg peaks with a forbidden AF magnetic intensity and a very weak nuclear one. The (2–11) Bragg peak fulfills these conditions. As shown in Fig. 5, its intensity increases below T_N, and this is a good indication for the validity of this scenario. Next, as the high-temperature ferroelectric distortion is mainly due to atomic displacements parallel to the c axis, the oxygen displacements proposed in this umbrella scenario should result at T_N in a slight change in the ferroelectric moment. Evidence for such an evolution has been recently reported in Ref. 20 thanks to high-resolution x rays and neutrons diffractions measurements. This result is another argument supporting our interpretation. Finally, the optical phonon spectrum is expected to exhibit anomalies at T_N but this remains, however, to be investigated.

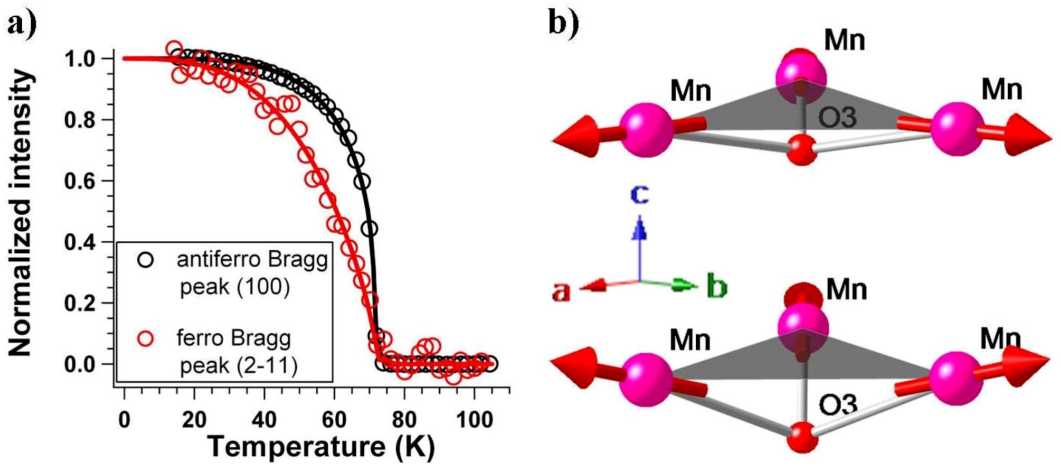

FIG. 7. (Color online) Umbrella scenario. (a) Left figure displays the temperature dependence of the (100) antiferromagnetic bragg peak and of the (2–11) Bragg peak (unpolarized neutron). The umbrella mechanism discussed in the text is sketched on the right panel (b). It evidences the existence of a small ferromagnetic component perpendicular to the manganese (Mn)-oxygen (O) layers when the oxygens are moving out of the plane.

VI. SUMMARY

In conclusion, polarized inelastic neutron-scattering experiments provide evidence for hybrid spin and lattice low-energy modes in $YMnO_3$ that can be considered as Goldstone modes of the multiferroic phase. The neutron polarization analysis directly shows their hybrid nature, revealing both spin and phononic counterparts. The mechanism responsible for this hybridization could be the Dzyaloshinskii interaction, in close analogy with the model recently proposed for orthorhombic multiferroic materials.

ACKNOWLEDGMENTS

We would like to thank Yvan Sidis and Claudine Lacroix for fruitful discussions. We acknowledge also support by the ANR-NEWTOM.

[1] M. Fiebig, J. Phys. D **38**, R123 (2005); M. Fiebig, Th. Lottermoser, D. Froehlich, A. V. Goltsev, and R. V. Pisarev, Nature (London) **419**, 818 (2002).
[2] J. Goldstone, Nuovo Cimento **19**, 154 (1961); J. Goldstone, A. Salam, and S. Weinberg, Phys. Rev. **127**, 965 (1962).
[3] S.-W. Cheong and M. Mostovoy, Nature Mater. **6**, 13 (2007).
[4] J. F. Scott, Science **315**, 954 (2007).
[5] H. Katsura, A. V. Balatsky, and N. Nagaosa, Phys. Rev. Lett. **98**, 027203 (2007).
[6] H. Katsura, N. Nagaosa, and A. V. Balatsky, Phys. Rev. Lett. **95**, 057205 (2005).
[7] M. Mostovoy, Phys. Rev. Lett. **96**, 067601 (2006).
[8] R. de Sousa and J. E. Moore, Phys. Rev. B **77**, 012406 (2008).
[9] V. G. Baryaktar and I. E. Chapius, Sov. Phys. Solid State **11**, 2628 (1970).
[10] I. A. Akhiezer and L. N. Davydov, Sov. Phys. Solid State **12**, 2563 (1971).
[11] A. Pimenov, A. A. Mukhin, V. Yu. Ivanov, V. D. Travkin, A. M. Balbashov, and A. Loidl, Nat. Phys. **2**, 97 (2006).
[12] R. Valdés Aguilar, A. B. Sushkov, Y. J. Choi, S.-W. Cheong, and H. D. Drew, Phys. Rev. B **77**, 092412 (2008).
[13] N. Kida, Y. Ikebe, Y. Takahashi, J. P. He, Y. Kaneko, Y. Yamasaki, R. Shimano, T. Arima, N. Nagaosa, and Y. Tokura, Phys. Rev. B **78**, 104414 (2008).
[14] A. B. Sushkov, R. V. Aguilar, S. Park, S. W. Cheong, and H. D. Drew, Phys. Rev. Lett. **98**, 027202 (2007).
[15] B. B. Van Aken, T. T. M. Palstra, A. Filippetti, and N. A. Spaldin, Nature Mater. **3**, 164 (2004).
[16] M. Cazayous, Y. Gallais, A. Sacuto, R. de Sousa, D. Lebeugle, and D. Colson, Phys. Rev. Lett. **101**, 037601 (2008).
[17] T. Katsufuji, M. Masaki, A. Machida, M. Moritomo, K. Kato, E. Nishibori, M. Takata, M. Sakata, K. Ohoyama, K. Kitazawa, and H. Takagi, Phys. Rev. B **66**, 134434 (2002).
[18] T. J. Sato, S. H. Lee, T. Katsufuji, M. Masaki, S. Park, J. R. D. Copley, and H. Takagi, Phys. Rev. B **68**, 014432 (2003).
[19] P. J. Brown and T. Chatterji, J. Phys.: Condens. Matter **18**, 10085 (2006).
[20] S. Lee, A. Pirogov, J. H. Han, K. H. Jang, M. Yonemura, T. Kamiyama, S. W. Cheong, F. Gozzo, N. Shin, H. Kimura, Y. Noda, and J. G. Park, Nature (London) **451**, 805 (2008); S. Lee, A. Pirogov, J. H. Han, J. G. Park, A. Hoshikawa, and T. Kamiyama, Phys. Rev. B **71**, 180413(R) (2005).
[21] R. M. Moon, T. Riste, and W. C. Koehler, Phys. Rev. **181**, 920 (1969).
[22] L. P. Régnault, in *Inelastic Neutron Polarization Analysis, Neutron Scattering from Magnetic Material*, edited by T. Chatterji (Elsevier, New York, 2006).
[23] S. Petit, F. Moussa, M. Hennion, S. Pailhés, L. Pinsard-Gaudart, and A. Ivanov, Phys. Rev. Lett. **99**, 266604 (2007). The NSF data taken at $H=0.15$ below and above T_N confirm the low-temperature splitting of the phonon's dispersion discussed in this reference.
[24] T. Chatterji, S. Ghosh, A. Singh, L. P. Regnault, and M. Rheinstadter, Phys. Rev. B **76**, 144406 (2007).
[25] W. B. Yelon, R. Scherm, and C. Vettier, Solid State Commun. **15**, 391 (1974).
[26] D. Senff, P. Link, K. Hradil, A. Hiess, L. P. Régnault, Y. Sidis, N. Aliouane, D. N. Argyriou, and M. Braden, Phys. Rev. Lett. **98**, 137206 (2007).
[27] A. Munoz, J. A. Alonso, M. J. Martinez-Lope, M. T. Casais, J. L. Martinez, and M. T. Fernandez-Diaz, Phys. Rev. B **62**, 9498 (2000).